International Journal of Nanomedicine

Dovepress
Taylor & Francis Group

Open Access Full Text Article

ORIGINAL RESEARCH

A Strategy to Design Non-Symmetric Compound by Modifying the End-Group Functional Atoms for Photothermal and Photodynamic Therapy of Tumor

Xin Xie[1,2,*], Jie Zeng[1,2,*], Miao-Yan Xu[1,2], Xin-Hao Han[1], Bing Fan[3], Xianglong Li[4], Duo-Duo Wei[1,2], Xiao-Jian Han[1,5], Shaorong Huang[1]

[1]Institute of Geriatrics, Jiangxi Provincial People's Hospital, the First Affiliated Hospital of Nanchang Medical College, Nanchang, Jiangxi, 330006, People's Republic of China; [2]School of Pharmacy, Jiangxi Medical College, Nanchang University, Nanchang, Jiangxi, 330006, People's Republic of China; [3]Department of Radiology, Jiangxi Provincial People's Hospital, The First Affiliated Hospital of Nanchang Medical College, Nanchang, Jiangxi, 330006, People's Republic of China; [4]Jiangxi Key Laboratory of Organic Chemistry, Institute of Organic Chemistry, Jiangxi Science & Technology Normal University, Nanchang, 330013, People's Republic of China; [5]The Second Department of Neurology, Jiangxi Provincial People's Hospital, the First Affiliated Hospital of Nanchang Medical College, Nanchang, Jiangxi, 330006, People's Republic of China

*These authors contributed equally to this work

Correspondence: Xiao-Jian Han; Shaorong Huang, Email hanxiaojian@hotmail.com; huangshaorong@ncmc.edu.cn

International Journal of Nanomedicine downloaded from https://www.dovepress.com/
For personal use only.

Background: The exploration of non-symmetric compound for combined photothermal therapy (PTT) and photodynamic therapy (PDT) in tumor treatment remains largely unexplored.

Methods: Through a molecular design strategy, a series of compound (Y-4Cl, Y-2Br, and Y-2Cl-Br) with fused - ring benzothiazole - pyrrole - thiophene - indenone constructure were synthesized to explore its phototherapy properties, to investigate their phototherapeutic properties, respectively. The non-symmetric compound Y-2Cl-Br was further formulated into nanoparticles (NPs) for detailed evaluation.

Results: The non-symmetric organic compound Y-2Cl-Br demonstrated a high molar extinction coefficient (ε) of 3.0×10^5 M^{-1} cm^{-1}. Y-2Cl-Br NPs exhibited exceptional photothermal performance, including a temperature increase (ΔT) of 34 °C and a photothermal conversion efficiency (PCE) of 61.2%. Additionally, Y-2Cl-Br NPs displayed superior photostability, a reactive oxygen species (ROS) generation efficiency 9.8-fold higher than indocyanine green (ICG), remarkable fluorescence imaging (FLI) capabilities, and excellent biocompatibility.

Conclusion: Both in vitro and in vivo studies confirmed that Y-2Cl-Br NPs are highly effective in PTT and PDT for tumor treatment, with minimal adverse effects. This work provides valuable insights into the design and application of non-symmetric organic compound photosensitizers (PSs) in cancer therapy.

Keywords: non-symmetric organic compound, photodynamic therapy, photothermal therapy, tumor

Introduction

Compared with surgery, radiotherapy and chemotherapy, phototherapy is a promising treatment method for tumors due to the advantages of minimal invasiveness, excellent spatiotemporal controllability, minimal toxic side effect and low drug resistance.[1–5] Phototherapy involves photothermal therapy (PTT) and photodynamic therapy (PDT) (Table S1), which plays an antitumor role by producing local high temperature[6–8] and toxic reactive oxygen species (ROS) to kill tumor cells.[9–11] In recent years, to promote the accuracy and efficacy of therapy, fluorescence imaging (FLI) is commonly used in guiding tumor therapy by determining the distribution and metabolism of the therapeutic agents to achieve real-time monitor.[12–14] Therefore, as an important part of phototherapy, the design of photosensitizer (PSs) with outstanding performance is crucial to the tumor therapy. However, the design of single PSs which simultaneously possessed PTT, PDT and FLI still faces massive challenge.

In the past several years, tremendous development had been achieved in PSs which mainly involved inorganic PSs and organic PSs.[15–18] Inorganic PSs including gold-based nanomaterials,[19,20] carbon-based nanostructures,[21,22] and other nanomaterials[23,24]

Received: 3 December 2024
Accepted: 25 March 2025
Published: 30 March 2025

© 2025 Xie et al. This work is published and licensed by Dove Medical Press Limited. The full terms of this license are available at https://www.dovepress.com/terms.php and incorporate the Creative Commons Attribution – Non Commercial (unported, v4.0) License (http://creativecommons.org/licenses/by-nc/4.0/). By accessing the work you hereby accept the Terms. Non-commercial uses of the work are permitted without any further permission from Dove Medical Press Limited, provided the work is properly attributed. For permission for commercial use of this work, please see paragraphs 4.2 and 5 of our Terms (https://www.dovepress.com/terms.php).

were used to tumor therapy due to the high performance in near-infrared (NIR) absorbance. However, the low biocompatibility of inorganic PSs greatly limited its application in tumor therapy. Luckily, organic PSs have much irreplaceable superior characteristics of the biodegradability, low mammalian toxicity, and flexible design.[25–28] Thus, enormous efforts have been made to develop highly efficient organic PSs. To date, some organic PSs have been approved by the US Food and Drug Administration (FDA) as clinical drugs such as indocyanine green (ICG),[29,30] while these organic PSs have some disadvantages such as poor photostability, single phototherapy mode[31,32] or poor light harvesting capability[33,34] and so on. Thus, to synthesize organic PSs with superior nature, non-symmetric organic compound has attracted great attention in the last decade (Table S2). Peng et al designed and synthesized non-symmetric organic compound called IR-Y6, which possessed high photothermal conversion effect (PCE) by rational manipulation of nonradiative decay channels.[35] Tang and Wang et al prepared the non-symmetric organic compound IDT-TPE with an order of magnitude higher ε to 8.9×10^4 m^{-1} cm^{-1}, which exhibited an extremely light harvesting capacity.[36] Meng et al modified the compound to obtain the new symmetric organic compound T780T-TPP-C_{12} possessing excellent photostability.[37] Tang et al designed and synthesized the symmetrical organic compound Y_5-2BO-2BTF by introducing a high-plane A-D-A skeleton with a high molar absorption coefficient of $1.0^6\times10^5$ M^{-1} cm^{-1} and a high photothermal conversion efficiency (77.8%).[38] Despite these PSs achieved excellent results, the design of most of the PSs were based on end-group symmetric compound[39,40] and the study on the aspect of the organic compound with non-symmetric end groups for PSs is still not reported.

Herein, we designed and synthesized the end-group symmetric compounds (Y-4Cl and Y-2Br) and end-group non-symmetric compounds (Y-2Cl-Br) with fused - ring benzothiazole - pyrrole - thiophene - indenone constructure to explore its phototherapy properties, respectively. Experimental results demonstrated Y-2Cl-Br had higher molar extinction coefficient (ε) of 3.0×10^5 $M^{-1}cm^{-1}$. After self-assembly of Y-2Cl-Br with DSPE-PEG_{2000}, Y-2Cl-Br nanoparticles (NPs) exhibited the highest temperature increase (ΔT) of 34 °C and PCE of 61.2% compared with the Y-4Cl NPs and Y-2Br NPs. Meanwhile, the Y-2Cl-Br NPs showed the strong ROS generation ability which was 9.8 folds of ICG. Given the superior performance in non-symmetric organic compound, Y-2Cl-Br NPs was selected as phototherapy agent for tumors. As expected, Y-2Cl-Br NPs showed good biocompatibility and outstanding antitumor efficacy both in vitro and in vivo (Scheme 1 and Figure S1). Collectively, this study illustrated that the design strategy of non-symmetric organic

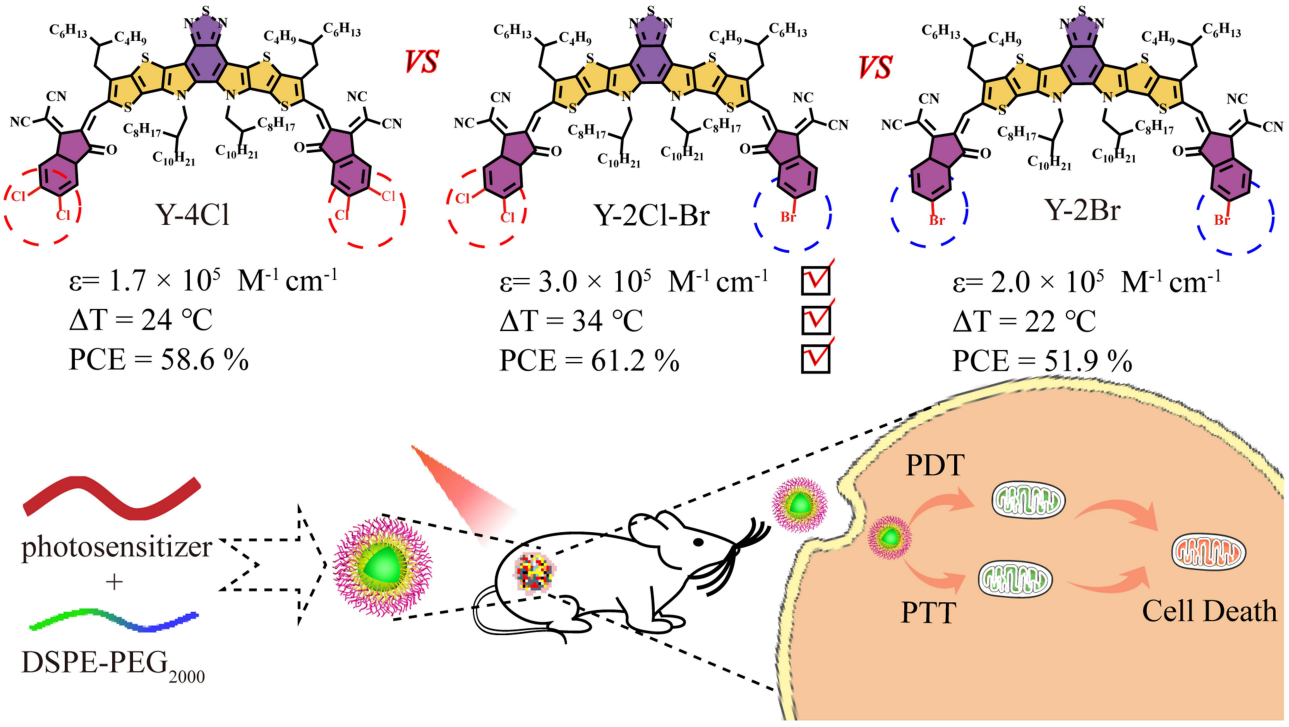

Scheme 1 Non-symmetric modified organic compound PSs for PTT and PDT of tumor.

compound is a possible ideal class of PSs for tumor therapy with excellent photothermal and photodynamic performance under FLI guidance.

Results and Discussion

The synthesis routes of the organic compounds Y-4Cl, Y-2Cl-Br, and Y-2Br were described in the Supporting Information (Figure S2). Their chemical structures were confirmed by nuclear magnetic resonance (NMR) (Figure S3–S5) and the curves of Y-4Cl, Y-2Cl-Br, and Y-2Br on the same graph (Figure S6). Matrix-Assisted Laser Desorption/Ionization Time of Flight Mass Spectrometry (MALDI-TOF-MS) (Figure S7−S9). To explore the difference in photophysical features between non-symmetric compound (Y-2Cl-Br) and symmetric compounds (Y-4Cl and Y-2Br), the light absorption ability was measured by the Ultraviolet-Visible Near-infrared (UV−VIS-NIR) spectrophotometer. The Y-4Cl, Y-2Cl-Br and Y-2Br exhibited the obvious absorption within 400 ~ 800 nm (Figure 1a) and the ε were determined as 1.7×10^5 $M^{-1}cm^{-1}$, 3.0×10^5 $M^{-1}cm^{-1}$ and 2.0×10^5 $M^{-1}cm^{-1}$, respectively (Figure S10–S12), which indicates the non-symmetric compounds possess the excellent light absorption. Subsequently, Y-4Cl, Y-2Cl-Br and Y-2Br were fabricated into Y-4Cl NPs, Y-2Cl-Br NPs and Y-2Br NPs by one-step nanoprecipitation method,[41,42] which effectively improved the biocompatibility and biostability. The final concentration of Y-4Cl NPs, Y-2Cl-Br NPs and Y-2Br NPs was determined by the standard curves of the absorbance of Y-4Cl, Y-2Cl-Br and Y-2Br in $CHCl_3$, respectively. Then, the photothermal property of Y-4Cl NPs, Y-2Cl-Br NPs and Y-2Br NPs were monitored under the same laser irradiation. As shown in Figure 1b–d and Figure S13, all three NPs had a certain temperature rise after irradiation. However, Y-2Cl-Br NPs showed the highest temperature increase (ΔT= 34 °C) compared with Y-4Cl NPs (ΔT= 24 °C) and Y-2Br NPs (ΔT= 22 °C). Finally, based on the reported method,[43,44] the PCE of Y-4Cl NPs, Y-2Cl-Br NPs and Y-2Br NPs were determined as 58.6%, 61.2% and 51.9% (Figure 1e and Figure S14), respectively. According to the results of ε, ΔT and PCE, the conclusion can be deduced that non-symmetric compound (Y-2Cl-Br) have a more excellent light absorption, ΔT as well as photothermal conversion capacity compared with symmetrical organic compounds (Y-4Cl and Y-2Br).

Due to the remarkable photophysical features, Y-2Cl-Br NPs have the great potential in tumor phototherapy. Therefore, we chose Y-2Cl-Br NPs as the tumor phototherapy agent. Firstly, the size and morphology of Y-2Cl-Br NPs were characterized by dynamic light scattering (DLS) and transmission electron microscopy. As shown in Figure 1f, the Y-2Cl-Br NPs had the uniform spherical morphology with a hydrodynamic diameter of around 128.1 nm. Considering the importance of biostability of NPs in tumor phototherapy, Y-2Cl-Br NPs were incubated in acid solution PBS which mimics the acidic properties in the tumor microenvironment, and assessed the changes in nanoparticle size. As displayed in Figure S15 and S16, the size of Y-2Cl-Br NPs almost was unchanged in acid solution PBS for 21 days. Besides, the size of Y-2Cl-Br NPs almost was unchanged in 1640 medium (10% FBS) for 14 days, suggesting excellent size stability (Figure S17). Furthermore, Y-2Cl-Br NPs retained the similar ΔT after five cool/heating cycles (Figure S18). These results indicate that Y-2Cl-Br NPs possess the excellent biostability for biological applications.

Based on the superior photothermal property of Y-2Cl-Br NPs + NIR, the photodynamic performance was further assayed. First, 1.3-Diphenylisobenzofuran (DPBF) was selected as a probe to examine the level of total ROS in cells (Figure S19). When the time extended to 90s after irradiation, the absorption intensity obviously decreased at 415 nm in DPBF + Y-2Cl-Br NPs + NIR (Figure 2a). However, the absorption intensity of DPBF + ICG + NIR had no significant change in the same way (Figure S20), suggesting Y-2Cl-Br NPs + NIR possessed the superior ROS production ability, which was 9.8 folds of ICG (Figure 2b). In addition, the ability of Y-4Cl NPs and Y-2Br NPs to generate ROS under 808 nm laser irradiation was also detected (Figure S21). However, among various photosensitizers of ICG, Y-2Cl-Br NPs, Y-2Br NPs and Y-4Cl NPs, Y-2Cl-Br NPs + NIR produced the most ROS in the same condition. To further verify the ROS generation capability of Y-2Cl-Br NPs + NIR, the SOSG, HPF and DHE were used to detect the ability to produce $^1O_2$, $^{\bullet}OH$ and $O_2^{\bullet -}$, respectively. As shown in Figure S22–S24, upon the NIR irradiation, compared with SOSG, APF and DHE alone, the curve of Y-2Cl-Br NPs + SOSG, Y-2Cl-Br NPs + HPF, Y-2Cl-Br NPs + DHE have gone up significantly. These results further indicated Y-2Cl-Br NPs + NIR possessed excellent PDT performance.

Next, we further distinguished the ROS categories in cells by using different fluorescence probes. The total ROS, $^1O_2$, $^{\bullet}OH$ and $O_2^{\bullet -}$ were detected by DCFH-DA, SOSG, HPF and DHE under both normoxic and hypoxic environment, respectively. Among them, the hypoxia environment is created by a three-gas incubator (1% O_2, 5% CO_2) (Figure S25). As shown in Figure 2c, under the normoxic environment, the images showed bright fluorescence signals in cells cultivated with Y-2Cl-Br NPs

https://doi.org/10.2147/IJN.S509789

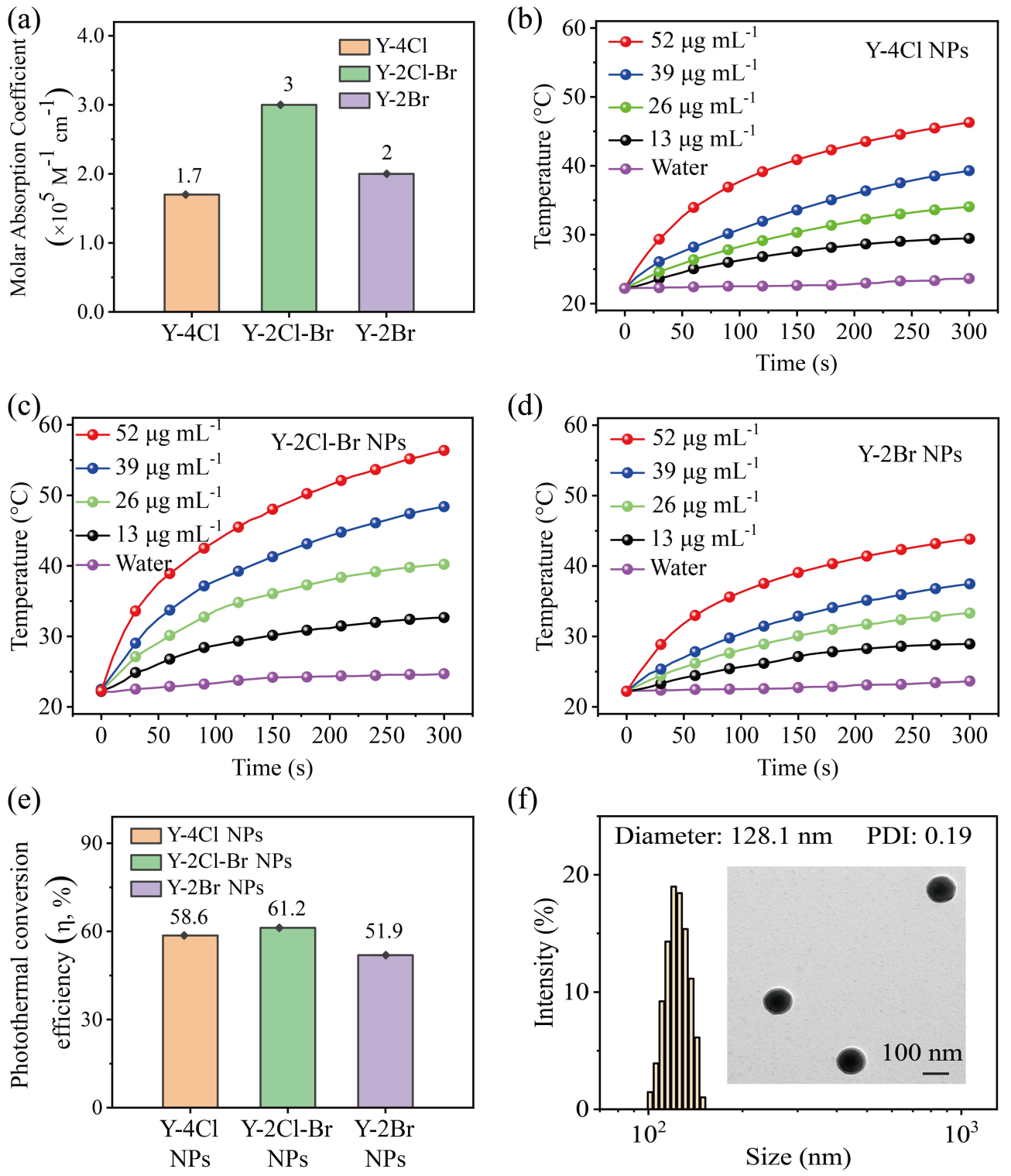

Figure 1 (**a**) Molar extinction coefficient of Y-4Cl, Y-2Cl-Br and Y-2Br. Photothermal property of Y-4Cl NPs (**b**), Y-2Cl-Br NPs (**c**) and Y-2Br NPs (**d**) at different concentrations (0, 13, 26, 39 and 52 μg mL^{-1}) under 808 nm laser irradiation (1.0 W cm^{-2}). (**e**) Photothermal conversion efficiency of Y-4Cl NPs, Y-2Cl-Br NPs and Y-2Br NPs. (**f**) DLS data of Y-2Cl-Br NPs (inset graph: transmission electron microscopy image of Y-2Cl-Br NPs; scale bar:100 nm).

and irradiated at 808 nm, indicating that Y-2Cl-Br NPs + NIR generated ROS, $^1O_2$, $^{\bullet}OH$ and $O_2^{\bullet -}$. However, under the hypoxic condition, $^{\bullet}OH$ and $O_2^{\bullet -}$ was still detected in cells treated with Y-2Cl-Br NPs + NIR suggesting Y-2Cl-Br NPs + NIR possessed type I PDT therapy ability. Besides, the 4T1 cell treated with Y-4Cl NPs + NIR and Y-2Br NPs + NIR also observed fluorescence

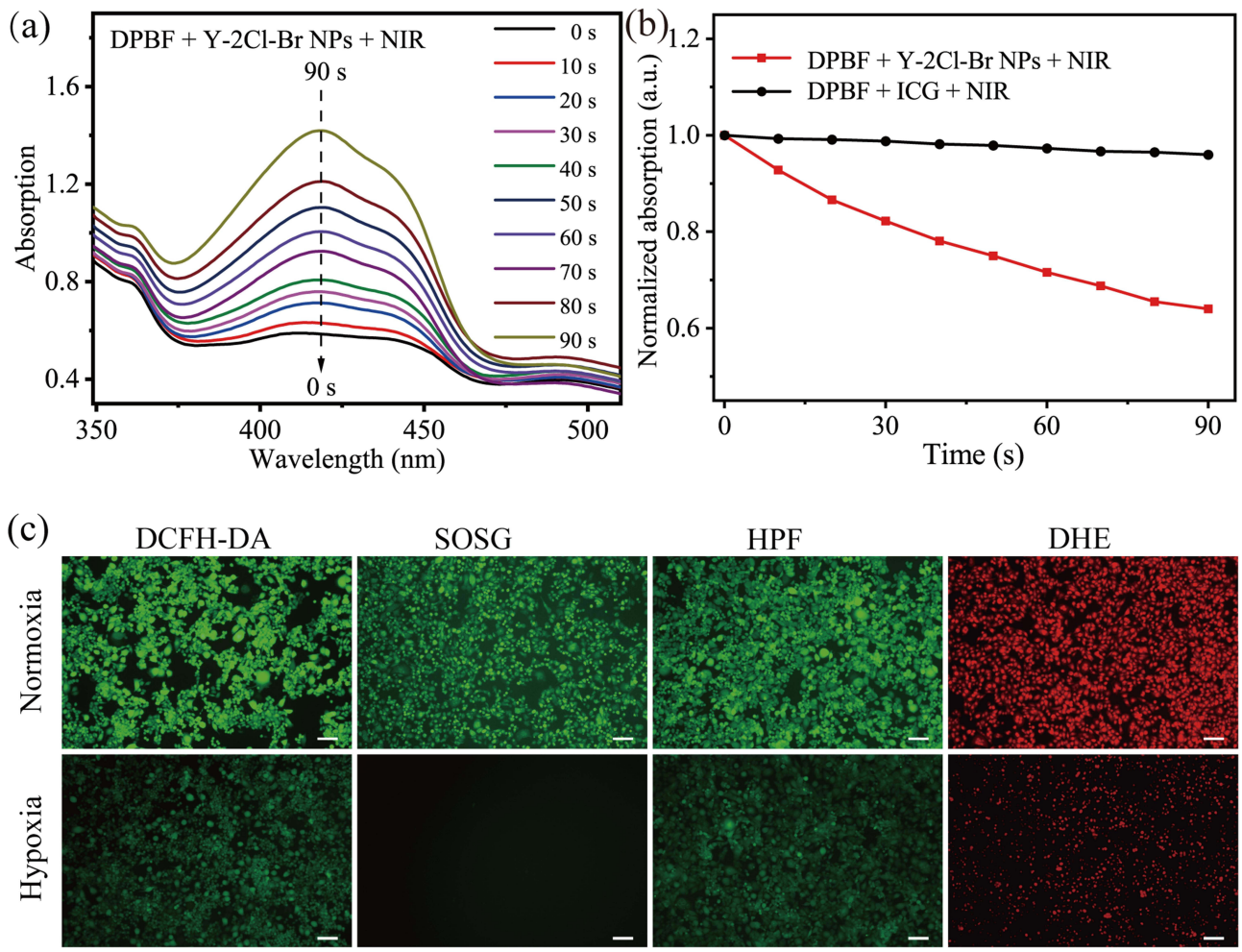

Figure 2 (**a**) ROS generation of Y-2Cl-Br NPs mixed with DPBF under laser irradiation (808 nm, 1.0 W cm^{-2}). (**b**) The changes in absorption of DPBF mixed with ICG or Y-2Cl-Br NPs solution at 415 nm. (**c**) Intracellular ROS in 4T1 cells treated with Y-2Cl-Br NPs + NIR under normoxia or hypoxia conditions. DCFH-DA, SOSG, HPF and DHE were used to detect total ROS, $^1O_2$, $^{\bullet}OH$ and $O_2^{\bullet-}$, respectively, scale bar: 100 μm.

signal, indicating Y-4Cl NPs and Y-2Br NPs possessed ability to generate ROS (Figure S26 and S27). On the contrary, no fluorescence signal was observed in cells treated with PBS, NIR and Y-2Cl-Br NPs, indicating intracellular ROS ($^1O_2$, $^{\bullet}OH$ and $O_2^{\bullet-}$) was not increased after these treatments (Figure S28). The above results demonstrate that Y-2Cl-Br NPs could be a superior photosensitizer for tumor PDT.

Due to the excellent photothermal and photodynamic performance of Y-2Cl-Br NPs under the 808 nm laser irradiation, we further assessed the antitumor effect in vitro. First, to detect the internalization of Y-2Cl-Br NPs in tumor cells, 4T1 cells was incubated with FITC-labeled Y-2Cl-Br NPs for different duration (0.5, 2, 4, 6 and 8 h) as the previous report.[45] As shown in Figure 3a, the fluorescence signal reached the strongest at 4 h, which demonstrated FITC-Y-2Cl-Br NPs could be efficiently internalized into tumor cells and provided an optimal time for phototherapy in vitro. Then, we used the Cell Counting Kit-8 (CCK-8) assays to evaluate the photodynamic and photothermal effects of Y-2Cl-Br NPs (0, 13, 26, 39 and 54 μg mL^{-1}) on 4T1 and B16F10 cells. Cell viability was dramatically decreased in both 4T1 and B16F10 cell lines after Y-2Cl-Br NPs + NIR. As shown in Figure 3b and c, cell viability was decreased to nearly 20.6% and 22.9% in 4T1 and B16F10 cells treated with 0 μg mL^{-1} ~ 39 μg $mL^{-1}$of Y-2Cl-Br NPs, respectively. Moreover, the cell viability was further decreased approximately 95% at the 52 μg mL^{-1} of Y-2Cl-Br NPs under the 808 nm (1.0 W cm^{-2}) irradiation. Besides, the cell ability of 4T1 and B16F10 cells still decreases at the power with 0.5 W cm^{-2} (Figure S29). And compared with ICG + NIR, Y-2Cl-Br NPs + NIR can kill more tumor cells (Figure S30). Meanwhile, under hypoxia, the cell viability of 4T1 cells also exhibited an apparent decrease after Y-2Cl-Br NPs + NIR (Figure S31). The above results show Y-2Cl-Br NPs + NIR

https://doi.org/10.2147/IJN.S509789

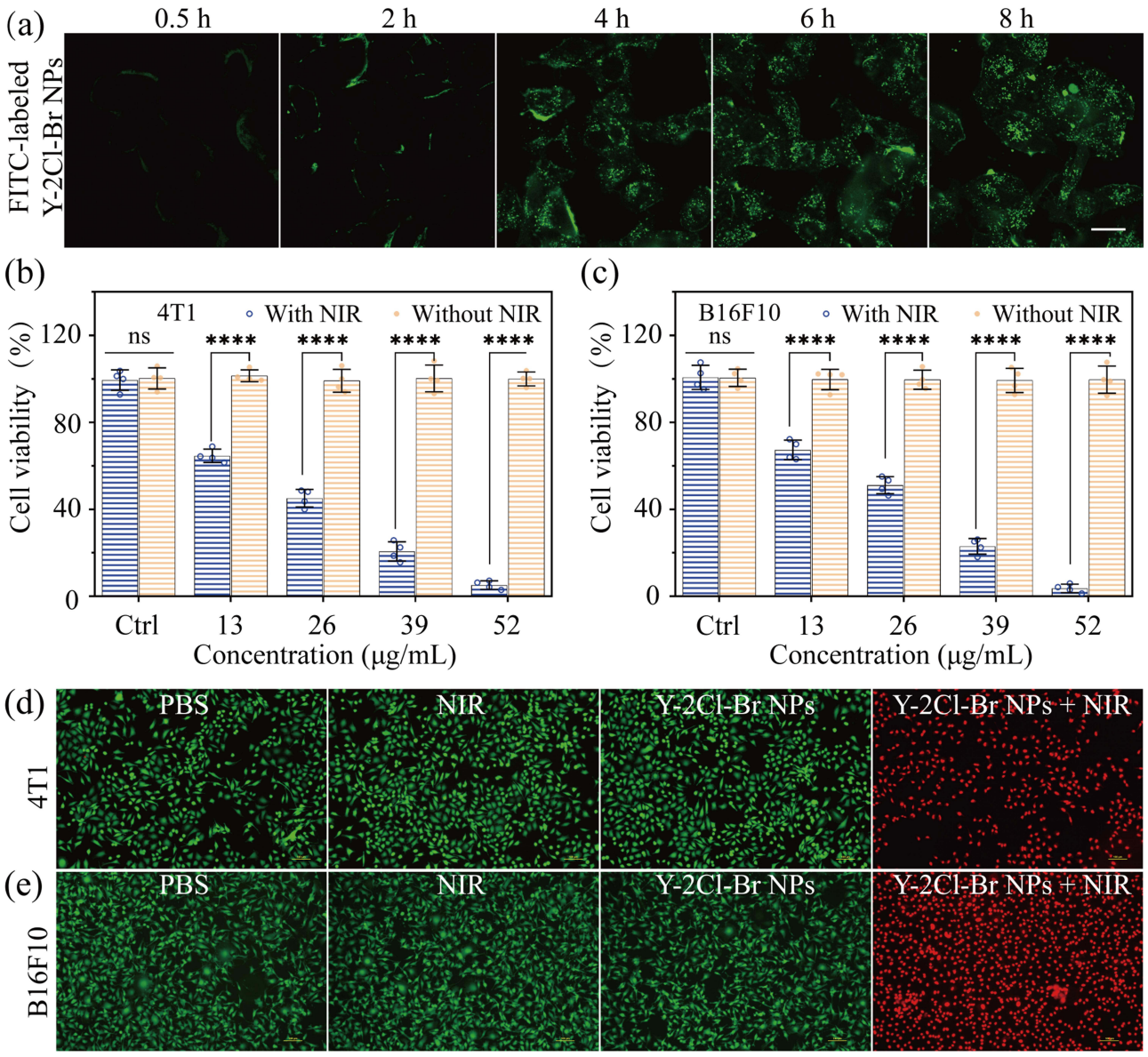

Figure 3 (**a**) The uptake efficiency of FITC-labeled Y-2Cl-Br NPs in 4T1 cells, scale bar: 20 μm. The viability of 4T1 (**b**) or B16F10 (**c**) cells incubated with Y-2Cl-Br NPs after different phototherapy modes. n = 4, "ns" means "no significance". ****$p < 0.0001$, *t*-test. The fluorescence images of 4T1 (**d**) and B16F10 (**e**) cells treated with PBS, NIR, Y-2Cl-Br NPs, and Y-2Cl-Br NPs + NIR after calcein AM (green)/propidium iodide (red) double-staining. Scale bar: 100 μm.

possesses a strong inhibitory effect on proliferation of tumor cells. In contrast, cell viability nearly maintained at 100% after treatment of Y-2Cl-Br NPs without NIR irradiation. The similar results were observed in H9c2, NIH 3T3 and HEK 293T cells without NIR irradiation (Figure S32). In addition, the antitumor effect of Y-2Cl-Br NPs + NIR was evaluated by calcein-AM (green fluorescence) and propidium iodide (red fluorescence) double staining to distinguish live and dead cells as previously reported.[46] As shown in Figure 3d and e, Figure S33 and S34, only bright green fluorescent was seen in the PBS, NIR or Y-2Cl-Br NPs treated 4T1 and B16F10 cells. Red fluorescence signal in dead cells was observed in the group with Y-2Cl-Br NPs + NIR. The result of live/dead double staining was consistent with the CCK-8 results. Subsequently, the flow cytometry analysis was conducted. As shown in Figure 4, cell apoptosis (85.77%) was significantly increased in Y-2Cl-Br NPs + NIR group compared with other groups (PBS, NIR and Y-2Cl-Br NPs) in 4T1 cells. Taken together, the results of CCK-8 assay, live/dead double staining and flow cytometry analysis indicated Y-2Cl-Br NPs + NIR possessed remarkable ability to ablate tumor cells.

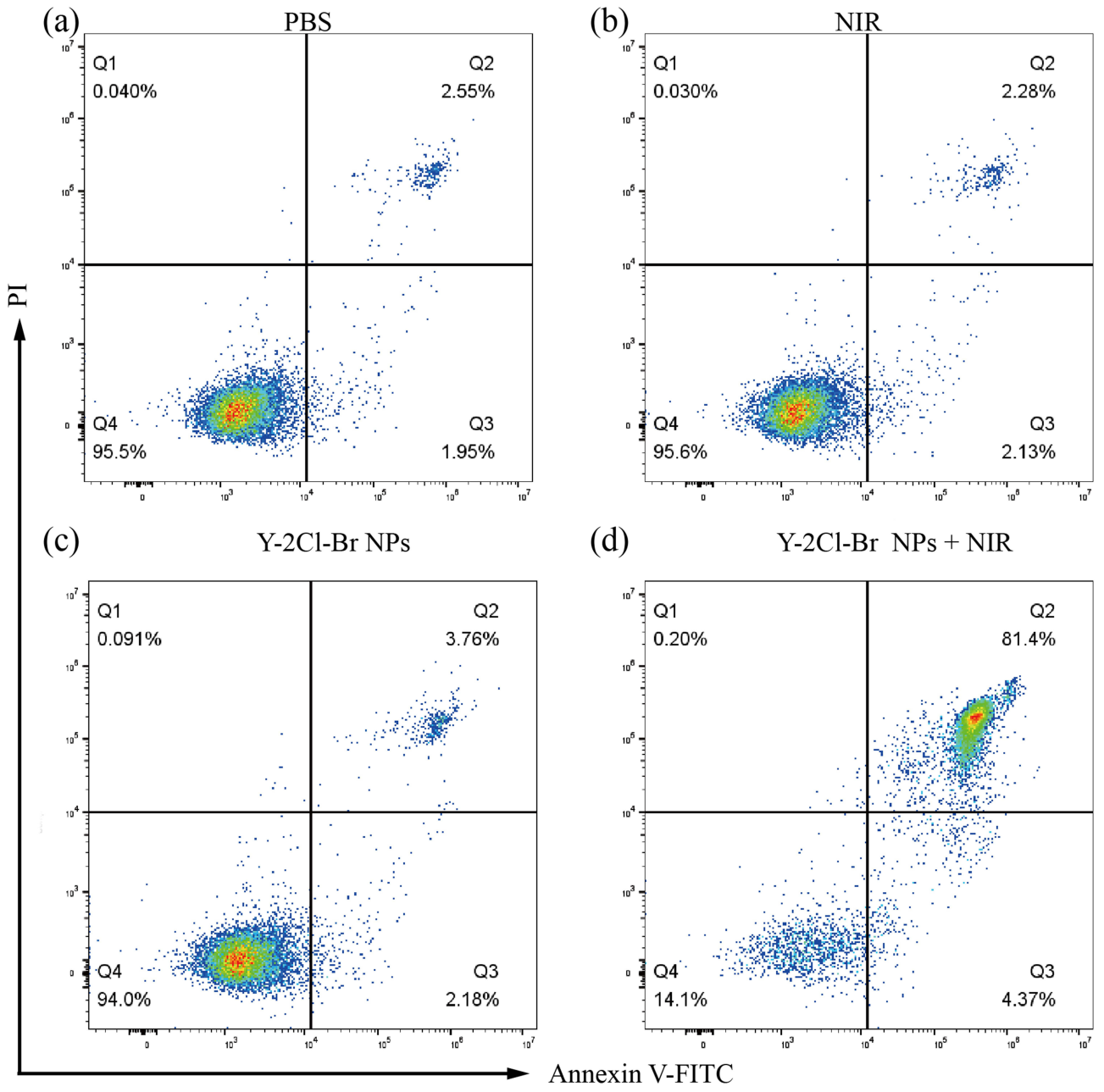

Figure 4 The results of flow cytometry were obtained from 4T1 cells stained with Annexin V-FITC/PI after treatment with (**a**) PBS, (**b**) NIR, (**c**) Y-2Cl-Br NPs or (**d**) Y-2Cl-Br NPs + NIR, respectively.

It is well known that mitochondria are the energy factories of the cell and involve in many other functions of the cellular activities. Considering the significance of mitochondria, we examined mitochondria function and morphology after different treatments. Firstly, Mito-SOX was employed to detect mitochondrial ROS in 4T1 cells as the previous. As displayed in Figure 5a, bright red fluorescence was observed in the group treated with Y-2Cl-Br NPs upon the 808 nm laser irradiation, demonstrating the increase of mitochondria ROS in Y-2Cl-Br NPs + NIR treated cells. To investigate whether the ROS and heat had an effect on mitochondria, the mitochondrial function and morphology in 4T1 cells was further assessed. JC-1 staining assay was conducted to detect mitochondrial membrane potential after different treatments as the previous reports. Green fluorescence signals of JC-1 in the group treated with Y-2Cl-Br NPs + NIR (Figure 5b) suggested the decrease of mitochondrial membrane potential and mitochondrial dysfunction. In addition, mitochondrial

https://doi.org/10.2147/IJN.S509789

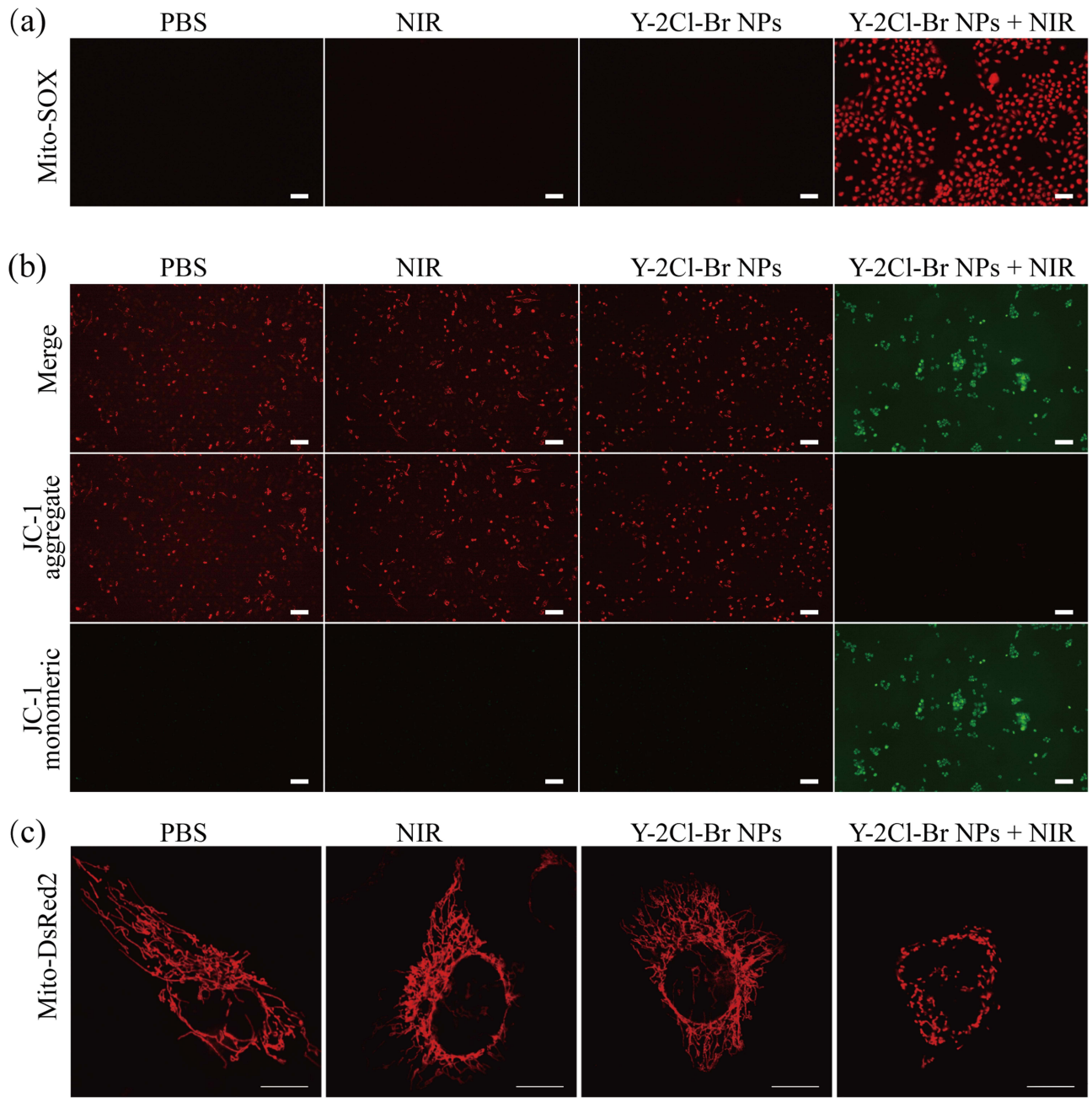

Figure 5 (**a**) Mitochondrial ROS in 4T1 cells treated with PBS, NIR, Y-2Cl-Br NPs or Y-2Cl-Br NPs + NIR, scale bar: 100 μm. (**b**) JC-1 staining of 4T1 cells treated with PBS, NIR, Y-2Cl-Br NPs or Y-2Cl-Br NPs + NIR, scale bar: 100 μm. (**c**) Mitochondrial morphology in 4T1 cells after different treatments, scale bar: 10 μm.

morphology was also monitored by transfection of Mito-DsReds2 in cells.[47] As shown in Figure 5c, the mitochondrial morphology in 4T1 cells treated with Y-2Cl-Br NPs was dot-like structures or fragmented network after 808 nm laser irradiation, while mitochondria in cells with the other treatments (PBS, NIR and Y-2Cl-Br NPs) was thread-like or tubular structures. These results suggested that Y-2Cl-Br NPs + NIR can cause mitochondrial dysfunction and structure breakdown and induce the death of tumor cells.

Furthermore, the in vivo anticancer performances were evaluated in 4T1 tumor-bearing mice. Firstly, we evaluated the hemocompatibility of Y-2Cl-Br NPs in vitro. The hemolysis ratios were less than 5% in red blood cells (RBCs) incubated with the mixture of Y-2Cl-Br NPs at different concentrations (0, 0.15, 0.3, 0.45 and 0.6 mg

mL^{-1}). Meanwhile, the supernatant of the RBCs suspension was clear (Figure S35). These results demonstrated the splendid hemocompatibility of Y-2Cl-Br NPs. Next, the FLI performance of Y-2Cl-Br NPs was also investigated both in vitro and in vivo. The in vitro fluorescence signal was shown in Figure S36, which showed the concentration-dependent relationship between fluorescence intensity and nanoparticle concentrations. To study the distribution and tumor accumulation of Y-2Cl-Br NPs in vivo, the Y-2Cl-Br NPs were intratumorally injected into 4T1-tumor-bearing BALB/c mice as the previous report.[48–50] Subsequently, the fluorescence images of mice were collected at 0, 3, 6, 9, 12 and 24 h postinjection (Figure S37a and b). The fluorescence signals from Y-2Cl-Br NPs at the tumor site reached the maximum value at 0 h postinjection, then followed by a gradual fluorescence decay because of the possible metabolism of Y-2Cl-Br NPs. To further assess the biodistribution of Y-2Cl-Br NPs in vivo, the major organs (heart, liver, spleen, lung and kidney) and tumors were isolated from the mice for FLI and quantitative analysis at 24 h postinjection. As illustrated in Figure S37c and d, the strong fluorescence signals in tumor tissue demonstrated the efficient accumulation of Y-2Cl-Br NPs. By contrast, no fluorescence signals were detected in the major organs. These results indicated that Y-2Cl-Br NPs can be served as a potential agent for tumor imaging guided phototherapy.

Based on the results above, we further evaluated the antitumor efficacy of Y-2Cl-Br NPs + NIR in the 4T1 tumor-bearing mice (Figure 6a). First, the 4T1 tumor-bearing mice were randomly divided into four groups: PBS, NIR, Y-2Cl-Br NPs and Y-2Cl-Br NPs + NIR. After different treatments, mice body weight, tumor relative volumes and variation in tumor site were recorded and monitored every three days. As shown in Figure 6b, no significant change in body weight was observed during the treatments, suggesting the low toxicity of Y-2Cl-Br NPs in vivo. From the observation of tumor site (Figure S38) and the measurement of tumor volume (Figure 6c), it was showed that the tumors in mice injected with PBS, NIR or Y-2Cl-Br NPs exhibited a rapid growth, while the tumor growth showed entirely ablation without recurrence in the mice treated with Y-2Cl-Br NPs + NIR. Furthermore, the tumors from all groups were collected (Figure 6d) and weighed (Figure 6e) at 14 days after the indicated treatments. The tumor completely disappeared in Y-2Cl-Br NPs + NIR group, which reached 100% tumor inhibition rate. Besides, hematoxylin and eosin (H&E) staining as well as Ki67 staining were used to assess antitumor effect. As displayed in Figure 6f, H&E staining revealed abundant nucleus absence and vacuolization in the Y-2Cl-Br NPs + NIR group, suggesting Y-2Cl-Br NPs + NIR can severely destruct tumor tissues. Meanwhile, Ki67 staining showed that the proliferation of tumor cells was significantly inhibited (Y-2Cl-Br NPs + NIR). These results illustrate that Y-2Cl-Br NPs + NIR can effectively suppress tumors growth in vivo, which suggests non-symmetric structure (Y-2Cl-Br) can be a promising photosensitizer for PTT/PDT of tumors.

To further assess the biosafety of photosensitizer, the biocompatibility of Y-2Cl-Br NPs was examined in vivo by blood routine test (Table S3), serum biochemical indexes (Table S4), and H&E staining of main organs from mice. Blood routine index including white blood cell (WBC) and red blood cell (RBC) counts had no significant difference between the Y-2Cl-Br NPs + NIR group and other treatment groups (Figure 7a and b). Moreover, the alanine aminotransferase (ALT), aspartate aminotransferase (AST), urea (UREA) and creatinine (CREA) (Figure 7c–f) also were within the normal range in all mice. Besides, H&E staining of major organs (heart, liver, spleen, lung and kidney) revealed the normal histological features without histological damage or inflammatory lesions in all groups (Figure 7g). The myocardial fibers of cardiomyocytes were pink, the nuclear structure was clear, and no obvious lesions were observed. The hepatic lobule structure was clear and complete, and the hepatic cord was empty. No obvious abnormality was found in the white pulp, red pulp and marginal area of spleen. The alveolar structure was intact, the alveolar cavity was empty, and no abnormal changes were observed in the lung interstitial. The normal glomerular structure was clear, the contour of the renal balloon was complete, and no obvious injury was observed. All these results indicated the excellent biocompatibility of Y-2Cl-Br NPs in tumor-bearing mice, highlighting its potential for clinical application of tumor PTT/PDT in the future.

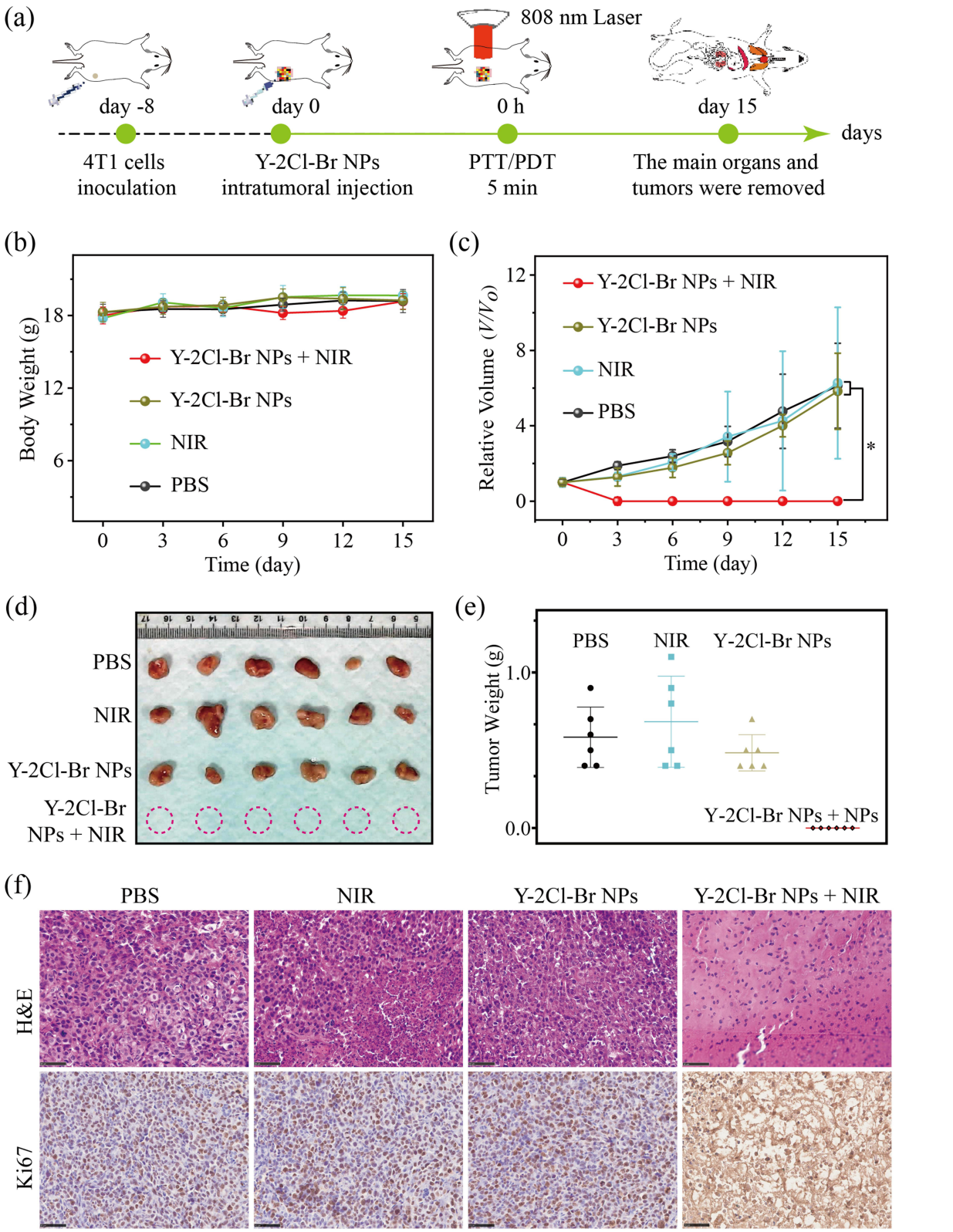

Figure 6 (**a**) Schematic diagram of Y-2Cl-Br NPs + NIR for the tumor therapy. (**b**) The changes in body weights of 4T1 tumor-bearing mice during the treatment process. (**c**) Relative tumor volume (V/V_0) in mice after different treatments. n=6, *$p < 0.05$, *t*-test. (**d**) The excised tumors and (**e**) weight of tumors from 4T1 tumor-bearing mice after different treatments in fifteenth day. (**f**) H&E and Ki67 staining analyses of tumor tissues. Scale bar: 100 μm.

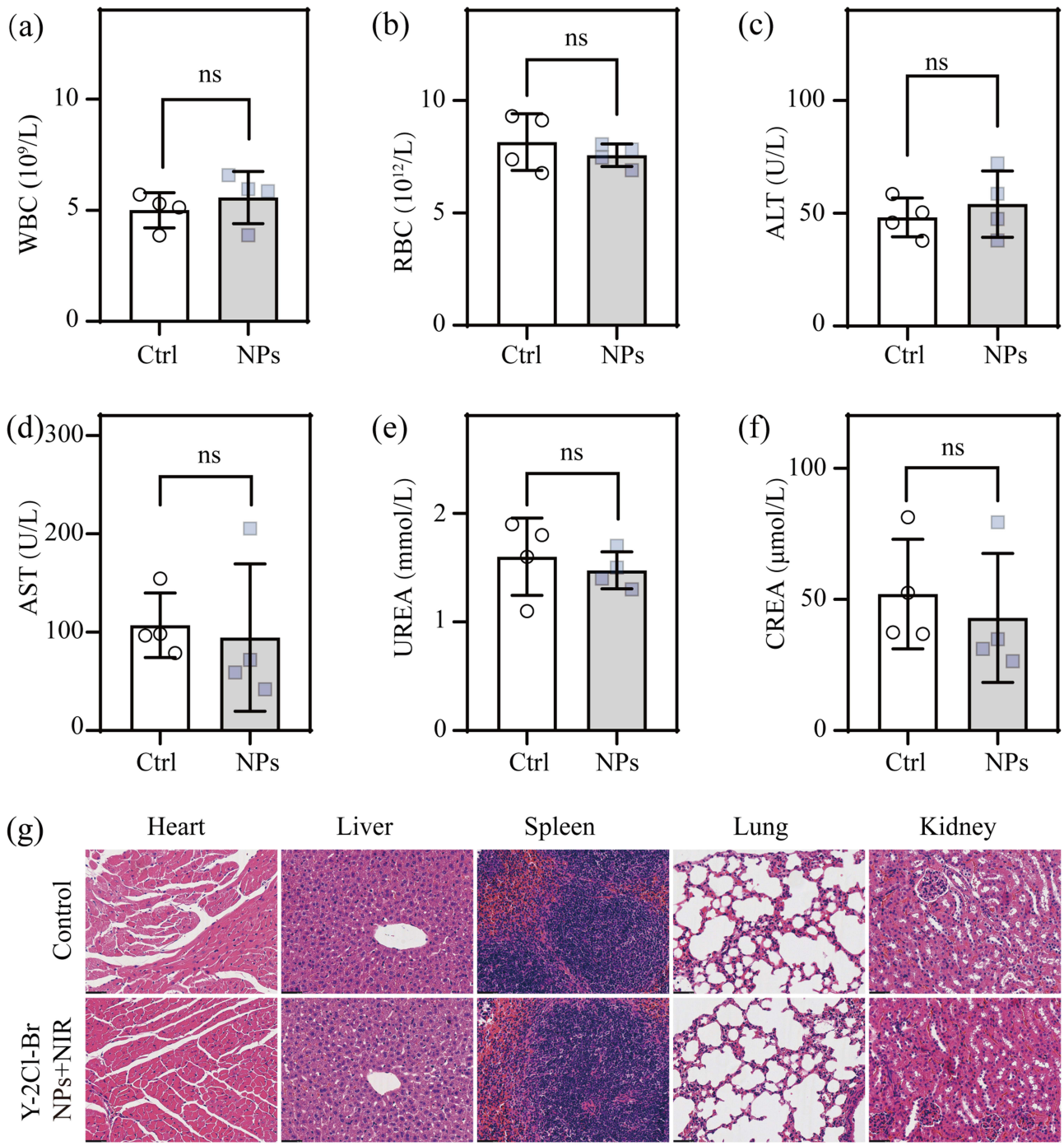

Figure 7 Blood routine parameters (**a**) WBC and (**b**) RBC, hepatic function markers (**c**) ALT, (**d**) AST, (**e**) UREA and (**f**) CREA as well as (**g**) H&E staining of major organs (heart, liver, spleen, lung and kidney) collected from health mice (saline) and mice treated with Y-2Cl-Br NPs + NIR. Scale bar: 50μm. n = 4, "ns" means "no significance".

Conclusions

In summary, we have designed and synthesized three organic compounds (Y-4Cl, Y-2Br and Y-2Cl-Br). The non-symmetric structure of Y-2Cl-Br possessed the most excellent performance (ε=3.0× 10^5 $M^{-1}cm^{-1}$). In addition, Y-2Cl-Br NPs also showed ΔT=34 °C, PCE=61.2% and 9.7-fold higher ROS generation efficiency than ICG. More importantly, benefiting from the admirable PTT and PDT capability, Y-2Cl-Br NPs guided by FLI exhibited completely tumor ablation ability with good biosafety. These results indicate that the design strategy of non-symmetric structure PSs offers a new avenue for antitumor study.

https://doi.org/10.2147/IJN.S509789

Ethics Approval and Consent to Participate

BALB/c female mice were purchased from GemPharmatech Co., Ltd (Nanjing, China) and cultured in accordance with the relevant standards of the Principles of Care for Experimental Animals. All animal experiments were approved by the Ethics Committee of Jiangxi Provincial People's Hospital (KT075) and that the mice treatments were performed in compliance with the Guide for the Care and Use of Laboratory Animals.

Consent for Publication

All authors agree to be published.

Acknowledgments

We thank the college of chemistry/institute of polymers and energy chemistry (IPEC), Nanchang University for materials testing.

Funding

The authors are grateful for the financial support from the National Natural Science Foundation of China (81472371), Natural Science Foundation of Jiangxi Provincial (20224ACB206014, 20242BAB20412), The Key Science and Technology Innovative Program of Jiangxi Health Commission (2023ZD001), the Science and Technology Research Project of Education Department of Jiangxi Province (GJJ2203553), Science and Technology Plan Project of Traditional Chinese Medicine of Jiangxi Province (2023A0148), Science and Technology Plan Project of Health Commission Jiangxi Province (202410166).

Disclosure

The authors declare no competing interests regarding the publication of this paper.

References

1. Li C, Jiang G, Yu J. et al. Fluorination Enhances NIR-II Emission and Photothermal Conversion Efficiency of Phototheranostic Agents for Imaging-Guided Cancer Therapy. *Adv Mater*. 2023;35(3):e2208229. doi:10.1002/adma.202208229
2. Fang L, Dai J, Wang X, et al. Glutathione-Driven Disassembly of Planar Organic Phototherapeutic Agents to Enhance Photodynamic-Photothermal Therapy Performance for Nasopharyngeal Carcinoma. *Small*. 2025;21(6):e2409196. doi:10.1002/smll.202409196
3. Sarbadhikary P, George BP, Abrahamse H. Recent Advances in Photosensitizers as Multifunctional Theranostic Agents for Imaging-Guided Photodynamic Therapy of Cancer. *Theranostics*. 2021;11(18):9054–9088. doi:10.7150/thno.62479
4. Liu N, Lin Q, Huang Z, et al. Mitochondria-Targeted Prodrug Nanoassemblies for Efficient Ferroptosis-Based Therapy via Devastating Ferroptosis Defense Systems. *ACS Nano*. 2024;18(11):7945–7958. doi:10.1021/acsnano.3c10133
5. Liang P, Huang X, Wang Y, et al. Tumor-Microenvironment-Responsive Nanoconjugate for Synergistic Anti vascular Activity and Phototherapy. *ACS Nano*. 2018;12(11):11446–11457. doi:10.1021/acsnano.8b06478
6. Zheng R, Zhao Q, Qing W, et al. Carrier-Free Delivery of Ultrasmall π-Conjugated Oligomer Nanoparticles with Photothermal Conversion over 80% for Cancer Theranostics. *Small*. 2022;18(4):e2104521. doi:10.1002/smll.202104521
7. Cui S, Pan X, Fan S, et al. A novel conjugated polymer synthesized via a noble metal-free catalyst in photothermal therapy of hepatocellular carcinoma mediated by second near-infrared (NIR-II) laser. *Mater Today Bio*. 2025;31:101488. doi:10.1016/j.mtbio.2025.101488
8. Sun P, Jiang X, Sun B, et al. Electron-acceptor density adjustments for preparation conjugated polymers with NIR-II absorption and brighter NIR-II fluorescence and 1064 nm active photothermal/gas therapy. *Biomaterials*. 2022;280:121319. doi:10.1016/j.biomaterials.2021.121319
9. Fan LF, Jian CJ, Li L, et al. A Bioactive Photosensitizer for Hypoxia-Tolerant Molecular Targeting-Photo-Immunotherapy of Malignant Tumor. *Adv Healthc Mater*. 2023;34:e2313755.
10. Feng L, Li C, Liu L, et al. Acceptor Planarization and Donor Rotation: a Facile Strategy for Realizing Synergistic Cancer Phototherapy via Type I PDT and PTT. *ACS Nano*. 2022;16(3):4162–4174. doi:10.1021/acsnano.1c10019
11. Marfavi Z, Cai Y, Lv Q, et al. The Synergy between Antibiotics and the Nanoparticle-Based Photodynamic Effect. *Nano Lett*. 2024;24:12973–12980.
12. Yuan Y, Feng Z, Li S, et al. Molecular Programming of NIR-IIb-Emissive Semiconducting Small Molecules for In Vivo High-Contrast Bioimaging Beyond 1500 nm. *Adv Mater*. 2022;34(19):e2201263. doi:10.1002/adma.202201263
13. Lei Z, Zhang F. Molecular Engineering of NIR-II Fluorophores for Improved Biomedical Detection. *Angew Chem Int Ed Engl*. 2021;60 (30):16294–16308. doi:10.1002/anie.202007040
14. Wang T, Wang S, Liu Z, et al. A hybrid erbium (III)-bacteriochlorin near-infrared probe for multiplexed biomedical imaging. *Nat Mater*. 2021;20 (11):1571–1578. doi:10.1038/s41563-021-01063-7
15. Chen L, Huang J, Tong M, et al. Photovoltaic Molecule-Based Phototheranostics With A-D-A Structure for Near-Infrared Fluorescence Imaging-Guided Synergetic Photodynamic and Photothermal Therapy of Tumors. *Luminescence*. 2024;39(10):e4930. doi:10.1002/bio.4930
16. Jiang Y, Jin Y, Feng C, et al. Engineering Hyaluronic Acid Microneedles Loaded with Mn2+ and Temozolomide for Topical Precision Therapy of Melanoma. *Adv Healthc Mater*. 2024;13(8):e2303215. doi:10.1002/adhm.202303215

17. Barman D, Rajamalli P, Bidkar AP, et al. Modulation of Donor in Purely Organic Triplet Harvesting AIE-TADF Photosensitizer for Image-guided Photodynamic Therapy. *Small*. 2025;21(7):e2409533. doi:10.1002/smll.202409533
18. Yang S, Sun B, Liu F, et al. NIR-II Imaging-Guided Mitochondrial-Targeting Organic Nanoparticles for Multimodal Synergistic Tumor Therapy. *Small*. 2023;19(26):e2207995. doi:10.1002/smll.202207995
19. Huang P, Rong P, Lin J, et al. Triphase interface synthesis of plasmonic gold bellflowers as near-infrared light mediated acoustic and thermal theranostics. *J Am Chem Soc*. 2014;136(23):8307–8313. doi:10.1021/ja503115n
20. Huang X, El-Sayed IH, Qian W, El-Sayed MA. Cancer cell imaging and photothermal therapy in the near-infrared region by using gold nanorods. *J Am Chem Soc*. 2006;128(6):2115–2120. doi:10.1021/ja057254a
21. Yan C, Shao X, Wang Y, et al. Multiexcitation Peaks and Multicolor Emission Nanoassemblies for Transmembrane Cell Imaging and Photoresponsivity Antibacterial. *ACS Appl Bio Mater*. 2024;7(8):5771–5779. doi:10.1021/acsabm.4c00855
22. Du X, Zhao C, Zhou M, et al. Hollow Carbon Nanospheres with Tunable Hierarchical Pores for Drug, Gene.; and Photothermal Synergistic Treatment. *Small*. 2017;13(6). doi:10.1002/smll.201602592
23. Wang X, Lv F, Li T, et al. Electrospun Micropatterned Nanocomposites Incorporated with Cu_2 S Nanoflowers for Skin Tumor Therapy and Wound Healing. *ACS Nano*. 2017;11(11):11337–11349. doi:10.1021/acsnano.7b05858
24. Liu T, Shi S, Liang C, et al. Iron Oxide Decorated MoS_2 Nanosheets with Double PEGylation for Chelator-Free Radiolabeling and Multimodal Imaging Guided Photothermal Therapy. *ACS Nano*. 2015;9(1):950–960. doi:10.1021/nn506757x
25. Teng KX, Niu LY, Kang YF, Yang QZ. Rational design of a "dual lock-and-key" supramolecular photosensitizer based on aromatic nucleophilic substitution for specific and enhanced photodynamic therapy. *Chem Sci*. 2020;11(35):9703–9711. doi:10.1039/D0SC01122C
26. Zhang X, Dou Y, Liu S, et al. Rationally Designed Benzobisthiadiazole-Based Covalent Organic Framework for High-Performance NIR-II Fluorescence Imaging-Guided Photodynamic Therapy. *Adv Healthc Mater*. 2024;13(17):e2303842. doi:10.1002/adhm.202303842
27. Chen X, Mendes BB, Zhuang Y, et al. A Fluorinated BODIPY-Based Zirconium Metal-Organic Framework for In Vivo Enhanced Photodynamic Therapy. *J Am Chem Soc*. 2024;146:1644–1656.
28. Cao W, Zhu Y, Wu F, et al. Three Birds with One Stone: acceptor Engineering of Hemicyanine Dye with NIR-II Emission for Synergistic Photodynamic and Photothermal Anticancer Therapy. *Small*. 2022;18(49):e2204851. doi:10.1002/smll.202204851
29. Xu G, Li C, Chi C, et al. A supramolecular photosensitizer derived from an Arene-Ru (II) complex self-assembly for NIR activated photodynamic and photothermal therapy. *Nat Commun*. 2022;13(1):3064. doi:10.1038/s41467-022-30721-w
30. Yang Y, Zhu W, Dong Z, et al. 1D Coordination Polymer Nanofibers for Low-Temperature Photothermal Therapy. *Adv Mater*. 2017;29:1.
31. Xiong H, Zhou K, Yan Y, Miller JB, Siegwart DJ. Tumor-Activated Water-Soluble Photosensitizers for Near-Infrared Photodynamic Cancer Therapy. *ACS Appl Mater Interfaces*. 2018;10(19):16335–16343. doi:10.1021/acsami.8b04710
32. Wang P, Kankala RK, Chen B, et al. Cancer Cytomembrane-Cloaked Prussian Blue Nanoparticles Enhance the Efficacy of Mild-Temperature Photothermal Therapy by Disrupting Mitochondrial Functions of Cancer Cells. *ACS Appl Mater Interfaces*. 2021;13(31):37563–37577. doi:10.1021/acsami.1c11138
33. Li S, Chang R, Zhao L, Xing R, van Hest JCM, Yan X. Two-photon nanoprobes based on bioorganic nanoarchitectonics with a photo-oxidation enhanced emission mechanism. *Nat Commun*. 2023;14(1):5227. doi:10.1038/s41467-023-40897-4
34. Zheng M, Zhao P, Luo Z, et al. Robust ICG theranostic nanoparticles for folate targeted cancer imaging and highly effective photothermal therapy. *ACS Appl Mater Interfaces*. 2014;6(9):6709–6716. doi:10.1021/am5004393
35. Gu H, Liu W, Zhen S, et al. "Internal and External Combined" Nonradiative Decay-Based Nanoagents for Photoacoustic Image-Guided Highly Efficient Photothermal Therapy. *ACS Appl Mater Interfaces*. 2021;13(39):46353–46360. doi:10.1021/acsami.1c14020
36. Li D, Li Y, Wu Q, et al. Add the Finishing Touch: molecular Engineering of Conjugated Molecule for High-Performance AIE Luminogen in Multimodal Phototheranostics. *Small*. 2021;17(37):e2102044. doi:10.1002/smll.202102044
37. Zhao X, Ma Y, Di J, et al. Synergetic Pyroptosis with Apoptosis Improving Phototherapy of Mitochondria-Targeted Cyanines with Superior Photostability. *ACS Appl Mater Interfaces*. 2024;16(10):12310–12320. doi:10.1021/acsami.3c19205
38. Yang S, Jia Q, Ou X, et al. Integration of Motion and Stillness: a Paradigm Shift in Constructing Nearly Planar NIR-II AIEgen with Ultrahigh Molar Absorptivity and Photothermal Effect for Multimodal Phototheranostics. *J Am Chem Soc*. 2025;147(4):3570–3583. doi:10.1021/jacs.4c15216
39. Jiang Z, Zhang C, Wang X, et al. A Borondifluoride-Complex-Based Photothermal Agent with an 80 % Photothermal Conversion Efficiency for Photothermal Therapy in the NIR-II Window. *Angew Chem Int Ed*. 2021;60(41):22376–22384. doi:10.1002/anie.202107836
40. Yang K, Long F, Liu W, et al. A-DA'D-A Structured Organic Phototheranostics for NIR-II Fluorescence / Photoacoustic Imaging-Guided Photothermal and Photodynamic Synergistic Therapy. *ACS Appl Mater Interfaces*. 2022;14(16):18043–18052. doi:10.1021/acsami.1c22444
41. Chen H, Zhang J, Chang K, et al. Highly absorbing multispectral near-infrared polymer nanoparticles from one conjugated backbone for photoacoustic imaging and photothermal therapy. *Biomaterials*. 2017;144:42–52. doi:10.1016/j.biomaterials.2017.08.007
42. Yuan B, Wu H, Wang H, Tang B, Xu JF, Zhang X. A Self-Degradable Supramolecular Photosensitizer with High Photodynamic Therapeutic Efficiency and Improved Safety. *Angew Chem Int Ed*. 2021;60(2):706–710. doi:10.1002/anie.202012477
43. Chen Y, He P, Jana D, et al. Glutathione-Depleting Organic Metal Adjuvants for Effective NIR-II Photothermal Immunotherapy. *Adv Mater*. 2022;34(21):e2201706. doi:10.1002/adma.202201706
44. Dong X, Liang J, Yang A, Qian Z, Kong D, Lv F. Fluorescence imaging guided CpG nanoparticles-loaded IR820-hydrogel for synergistic photothermal immunotherapy. *Biomaterials*. 2019;209:111–125. doi:10.1016/j.biomaterials.2019.04.024
45. Chen PF, Qu F, Chen SY, et al. Bandgap Modulation and Lipid Intercalation Generates Ultrabright D–A–D-Based Zwitterionic Small-Molecule Nanoagent for Precise NIR-II Excitation Phototheranostic Applications. *Adv Healthc Mater*. 2022;32:e2208463.
46. Shi K, Liu X, Liu Y, Liu C, Wang Y, Liu Y. Supramolecular Polypeptide Self-Assembly Mediated in Situ Elicitation of Robust Innate and Adaptive Immune Responses Boosts Immunogenic Photothermal Therapy toward "Cold. *Tumor Adv Healthc Mater*. 2023;12(2):e2202017. doi:10.1002/adhm.202202017
47. Xie X, Wang K, Zeng J, et al. A novel polymer enabled by polymerized small molecule strategy for tumor photothermal and photodynamic therapy. *J Nanobiotechnology*. 2023;21(1):497. doi:10.1186/s12951-023-02272-9
48. Yu J, Xu J, Jiang R, et al. Versatile chondroitin sulfate-based nanoplatform for chemo-photodynamic therapy against triple-negative breast cancer. *Int J Biol Macromol*. 2024;265(Pt 1):130709. doi:10.1016/j.ijbiomac.2024.130709

49. Wan Y, Lu G, Wei WC, et al. Stable Organic Photosensitizer Nanoparticles with Absorption Peak beyond 800 Nanometers and High Reactive Oxygen Species Yield for Multimodality Phototheranostics. *ACS Nano*. 2020;14(8):9917–9928. doi:10.1021/acsnano.0c02767
50. Yu D, Wang Y, Chen J, et al. Co-delivery of NIR-II semiconducting polymer and pH-sensitive doxorubicin-conjugated prodrug for photothermal/chemotherapy. *Acta Biomater*. 2022;137:238–251. doi:10.1016/j.actbio.2021.10.009

International Journal of Nanomedicine

Dovepress
Taylor & Francis Group

Publish your work in this journal

The International Journal of Nanomedicine is an international, peer-reviewed journal focusing on the application of nanotechnology in diagnostics, therapeutics, and drug delivery systems throughout the biomedical field. This journal is indexed on PubMed Central, MedLine, CAS, SciSearch®, Current Contents®/Clinical Medicine, Journal Citation Reports/Science Edition, EMBase, Scopus and the Elsevier Bibliographic databases. The manuscript management system is completely online and includes a very quick and fair peer-review system, which is all easy to use. Visit http://www.dovepress.com/testimonials.php to read real quotes from published authors.

Submit your manuscript here: https://www.dovepress.com/international-journal-of-nanomedicine-journal